$(Sr_3N)E$ and $(Ba_3N)E$ (E = Sb, Bi): Synthesis, Crystal Structures, and Physical Properties

Frank Gäbler, Martin Kirchner, Walter Schnelle, Ulrich Schwarz, Miriam Schmitt, Helge Rosner, and Rainer Niewa*

Dresden, Max-Planck-Institut für Chemische Physik fester Stoffe

Received May 24th, 2004.

Dedicated to Professor Martin Jansen on the Occasion of his 60th Birthday

Abstract. Single phase powders of $(Sr_3N)Sb$, $(Sr_3N)Bi$ ($Pm\bar{3}m$, No. 221, $Z = 1$, Sb: $a = 517.25(2)$ pm, $V = 138.390(8) \cdot 10^6$ pm^3, Bi: $a = 520.691(8)$ pm, $V = 141.170(4) \cdot 10^6$ pm^3), $(Ba_3N)Sb$, and $(Ba_3N)Bi$ ($P6_3/mmc$, No. 194, $Z = 2$, Sb: $a = 753.33(3)$ pm, $c = 664.45(3)$ pm, $V = 326.56(2) \cdot 10^6$ pm^3, Bi: $a = 761.28(4)$ pm, $c = 668.05(3)$ pm, $V = 335.30(2) \cdot 10^6$ pm^3) were obtained from reactions of melt beads of the respective elements with bulk compositions of A_3E (A = Sr, Ba; E = Sb, Bi) in nitrogen atmosphere of ambient pressure at $T = 1070$ K (Sr) and $T = 1120$ K (Ba). The compositions were derived from chemical analyses and supported by Rietveld refinements based on powder X-ray diffraction patterns. The Sr containing compounds crystallize in the cubic anti-perovskite type arrangement, the Ba containing compounds in the hexagonal anti-$BaNiO_3$ structure type. Magnetic susceptibility and electrical resistivity data indicate that the compounds are diamagnetic semiconductors. The optical band gaps of $(Sr_3N)Sb$ and $(Sr_3N)Bi$ were determined by diffuse reflectivity to 1.15 eV and 0.89 eV, respectively. The experimental results are in agreement with electronic structure calculations. Chemical bonding is characterized in a simplified picture as ionic with significant orbital mixing.

Keywords: Nitrides; Antimony; Bismuth; Perovskites; Crystal structures; Magnetic properties; Electrical resistivity; Electronic structure calculations

$(Sr_3N)E$ und $(Ba_3N)E$ (E = Sb, Bi): Synthese, Kristallstrukturen und physikalische Eigenschaften

Inhaltsübersicht. $(Sr_3N)Sb$, $(Sr_3N)Bi$ ($Pm\bar{3}m$, Nr. 221, $Z = 1$, Sb: $a = 517{,}25(2)$ pm, $V = 138{,}390(8) \cdot 10^6$ pm^3, Bi: $a = 520{,}691(8)$ pm, $V = 141{,}170(4) \cdot 10^6$ pm^3), $(Ba_3N)Sb$, und $(Ba_3N)Bi$ ($P6_3/mmc$, Nr. 194, $Z = 2$, Sb: $a = 753{,}33(3)$ pm, $c = 664{,}45(3)$ pm, $V = 326{,}56(2) \cdot 10^6$ pm^3, Bi: $a = 761{,}28(4)$ pm, $c = 668{,}05(3)$ pm, $V = 335{,}30(2) \cdot 10^6$ pm^3) wurden als phasenreine Pulver durch Reaktionen von Schmelzperlen der Zusammensetzungen A_3E (A = Sr, Ba; E = Sb, Bi) mit Stickstoff bei Temperaturen von $T = 1070$ K (Sr) und $T = 1120$ K (Ba) erhalten. Die Zusammensetzungen der Verbindungen wurde durch chemische Analysen bestimmt und mit Ergebnissen aus Rietveldverfeinerungen an Röntgenpulverdiffraktogrammen unterstützt. Die Sr-Verbindungen kristallisieren im Strukturtyp des kubischen (anti-)Perowskits, die Ba-Verbindungen im hexagonalen (anti-)$BaNiO_3$-Typ. Messungen der magnetischen Suszeptibilitäten und elektrischen Widerstände deuten auf das Vorliegen von diamagnetischen Halbleitern. An $(Sr_3N)Sb$ und $(Sr_3N)Bi$ wurden die optischen Bandlücken durch diffuse Reflexion zu 1,15 eV und 0.89 eV bestimmt. Die experimentellen Befunde sind in Übereinstimmung mit Ergebnissen aus Berechnungen der elektronischen Struktur. Die chemische Bindung wird in einem vereinfachten Bild als ionogen mit signifikanten Beiträgen durch Mischung von Orbitalen beschrieben.

Introduction

Due to the outstanding properties of some binary nitrides and their growing technical importance, ternary and higher nitrides have raised considerable interest over the last decade [1-3]. Ternary nitrides with the general formula $(Ca_3N)E$ (E = Tl, Ge, Sn, Pb, P, As, Sb, Bi, Au) are already known for a couple of years [4-6]. They crystallize in a cubic anti-perovskite structure type (E = P, As distorted to an orthorhombic crystal structure) and exhibit interesting trends: Assuming calcium and nitrogen to form ions Ca^{2+} and N^{3-}, respectively, one can achieve - within the same structure type - various electronic situations, from an electron excess as in $(Ca_3N)Au$ (formally $(Ca^{2+})_3N^{3-}Au^- \cdot 2e^-$) [4], via compounds $(Ca_3N)E$ ($E = P^{3-}$, As^{3-}, Sb^{3-}, Bi^{3-}) [5], which obey the octet rule, to an electron deficiency as in $(Ca_3N)Tl$ [6]. This change of the electronic situation is mirrored by the physical behavior of the compounds: $(Ca_3N)Au$ represents an electrical conductor, whereas the group 15 compounds are insulators or semiconductors (E = Sb, Bi). Similarly, the cubic anti-perovskites $(Mg_3N)E$ with E = As and Sb are yellow insulators and black semiconductors, respectively [7]. The corresponding group 14 compounds are discussed in terms of electron deficient metals of the composition $(Ca_3N)E$ (E = Ge, Sn, Pb) [5, 8].

* Dr. R. Niewa
Max-Planck-Institut für Chemische Physik fester Stoffe,
Nöthnitzer Str. 40
D-01187 Dresden
Fax: +49 (0) 351 4646 3002
email: niewa@cpfs.mpg.de

  DOI: 10.1002/zaac.200400256

Anti-perovskite oxides are only known with group 14 elements $(A_3O)E$ (A = Ca, Sr, Ba, E = Si, Ge, Sn, Pb) [9−12]. Associated to the observation of generally larger band gaps of oxides compared to nitrides these can be obtained as colorless insulators. These experimental findings and the electronic and structural properties have raised considerable interest in theoretical studies of the electronic structures and high pressure investigations of the crystal structures of these compounds [6, 8, 13−16].

Only few ternary nitrides with E = Sb, Bi are known. Previously reported were the cubic anti-perovskites $(Mg_3N)Sb$ [7], $(Ca_3N)E$ [5], and $(Mn_3N)Sb$ [17], and the compounds $(U_2N_2)E$ [18], and $(Th_2N_2)E$ [18]. No ternary nitrides of Sb or Bi with A = Sr, Ba are known so far.

Experimental Section

All manipulations were carried out in an argon filled glove box ($p(O_2, H_2O)$ < 0.1 ppm). For preparation of single phase samples antimony or bismuth (Chempur, 99.999 %) and strontium or barium (Alfa Aesar, 99.9 %) were fused in an arc furnace (molar ratio 1 : 3, typically 2 g sample) operated in argon (Messer-Griesheim, 99.999 %, additionally purified by passing over molsieve, Roth 3 Å, and BTS-catalyst, Merck). No phases A_3E with A = Sr, Ba; E = Sb, Bi are known according to the phase diagrams [19]; X-ray powder diffraction patterns indicated the presence of A_2E as main phases. In a second step the metallic regulus was heated under nitrogen of ambient back-pressure (Messer-Griesheim, 99.999 %, additionally purified as described for argon) to a maximum temperature of T = 1070 K for Sr containing samples and T = 1120 K for Ba containing beads. This approach leads to better results than solid state sinter reactions of binary nitrides AN_x with melt beads A_xE of appropriate compositions in Ar atmosphere or sealed ampoules. The reaction temperatures with nitrogen were taken from DTA/TG experiments. All compounds were obtained as gray powders, which are sensitive against water and moisture.

Chemical analyses on O and N were carried out using the carrier gas hot-extraction technique on a LECO analyzer TCH-600. Quantitative analyses of the A = Sr, Ba and E = Sb, Bi constituents were performed using an ICP-OES (Varian Vista RL). All values are averages of at least 3 independent measurements:

$(Sr_3N)Sb$: $w(Sr)$ = 65.8(9) %, $w(Sb)$ = 30.5(5) %, $w(N)$ = 3.2(2) %, $w(O)$= 0.24(1) %, i. e. $(Sr_{3.00(4)}N_{0.92(4)}O_{0.060(2)})Sb_{1.00(2)}$
$(Ba_3N)Sb$: $w(Ba)$ = 74.3(3) %, $w(Sb)$ = 23.8(4) %, $w(N)$ = 2.61(4) %, $w(O)$ < 0.10 %, i. e. $(Ba_{3.00(3)}N_{0.89(2)})Sb_{1.09(2)}$
$(Sr_3N)Bi$: $w(Sr)$ = 52.6(5) %, $w(Bi)$ = 44.2(3) %, $w(N)$ = 2.7(1) %, $w(O)$= 0.16(1) %, i. e. $(Sr_{3.00(3)}N_{0.97(4)}O_{0.050(3)})Bi_{1.060(5)}$
$(Ba_3N)Bi$: $w(Ba)$ = 64.6(7) %, $w(Bi)$ = 32.8(5) %, $w(N)$ = 2.06(5) %, $w(O)$ = 0.13(1) %, i. e. $(Ba_{3.00(3)}N_{0.94(3)}O_{0.040(4)})Bi_{1.00(1)}$

DTA/TG-measurements were performed using a STA 449C analyzer (Ar- or N_2-atmosphere purified as described above, thermocouple type S, NETZSCH Gerätebau, Selb) completely integrated into a glove box to avoid any sample hydrolysis. Temperature calibration was obtained using 5 melting standards in the temperature range of 370 K ≤ T ≤ 1470 K.

The ternary nitrides were characterized by X-ray powder diffraction using an Imaging Plate Guinier Camera (HUBER diffraction, Cu$K\alpha_1$ radiation, 4·15 min scans, 8° ≤ 2Θ ≤ 100°). The samples were loaded between two polyimide foils in an aluminum cell with a rubber sealing to exclude any moisture. Comparison of the powder patterns of the first and the final scan did not indicate significant hydrolysis during the measurement procedure. The hexagonal structures of $(Ba_3N)E$ (E = Sb, Bi) were refined on the basis of powder X-ray diffraction patterns (program package FULLPROF [20]).

The magnetic susceptibility of powder samples (sealed in silica tubes, 400 mbar He) was measured in a SQUID magnetometer (MPMS XL-7, Quantum Design) in external magnetic fields ranging from 70 kOe to 20 Oe between 1.8 K and 400 K. Measurements of the electrical resistivity were performed on powders pressed in a sapphire die in a four contact dc van-der-Pauw set-up between 4 K and 320 K.

The optical band gap was determined from diffuse reflection (Cary 500, praying mantis, white standard $BaSO_4$, ratio 5 : 1) under inert conditions. The absorption energy was taken as the inflection point of the step-like decrease of the diffuse reflectivity.

Calculations

To investigate the electronic structures of $(Sr_3N)E$ and $(Ba_3N)E$ (E= Sb, Bi) a full potential non-orthogonal local-orbital scheme (FPLO) [21] within the local density approximation (LDA) was applied. In the scalar relativistic calculations the exchange and correlation potential of *Perdew* and *Wang* [22] was used. As basis sets, N(2*s*, 2*p*, 3*d*), Sr(4*s*, 4*p*, 5*s*, 5*p*, 4*d*), Ba(5*s*, 5*p*, 6*s*, 6*p*, 5*d*), Sb(4*s*, 4*p*, 4*d*, 5*s*, 5*p*, 5*d*) and Bi(5*s*, 5*p*, 5*d*, 6*s*, 6*p*, 6*d*) states were taken into account. All lower lying states were calculated as core states that are treated fully relativistically. The N(3*d*), Sr(4*d*), Ba(5*d*) states as well as the Bi(6*d*) states were taken into account as polarization states to increase the completeness of the basis set. The inclusion of the Sr(4*s*, 4*p*), Ba(5*s*, 5*p*), Sb(4*s*, 4*p*, 4*d*) and Bi(5*s*, 5*p*, 5*d*) semi-core like states in the valence was necessary to account for non-negligible core-core overlaps. The spatial extension of the basis orbitals, controlled by a confining potential $(r/r_0)^4$ [23], was optimized to minimize the total energy. A k-mesh of 396 (407) points in the irreducible part of the Brillouin zone of the cubic (hexagonal) structures was used to ensure accurate density of states and band structure information. All calculations have been carried out for the experimentally observed structural data.

Results and Discussion

The optimal preparation conditions for ternary nitrides $(A_3N)E$ (A = Sr, Ba; E = Sb, Bi) from mixtures of the metals or their binary compounds in nitrogen atmosphere were derived from extensive DTA/TG investigations. The TG curve (heating rate 10 K/min) of, e. g., 'Sr_3Sb' in nitrogen atmosphere is interpreted according to the binary phase diagram Sr−Sb [19] as follows (figure 1): a significant weight gain starts at about T = 770 K. At the eutectic temperature of the system Sr_2Sb−Sr of T = 985 K the weight increases steeply and is accompanied by an exothermic heat effect which almost completely covers the endothermic heat signal of the eutectic. Under the given conditions the weight

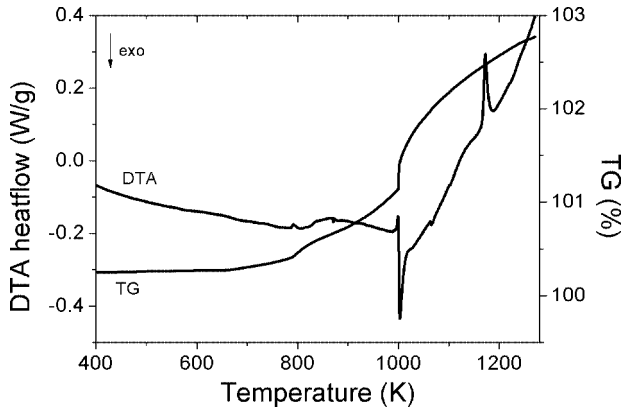

Figure 1 Simultaneous DTA/TG measurement of the reaction of melt beads of the general composition of 'Sr_3Sb' with nitrogen (heating rate 10 K/min) forming $(Sr_3N)Sb$.

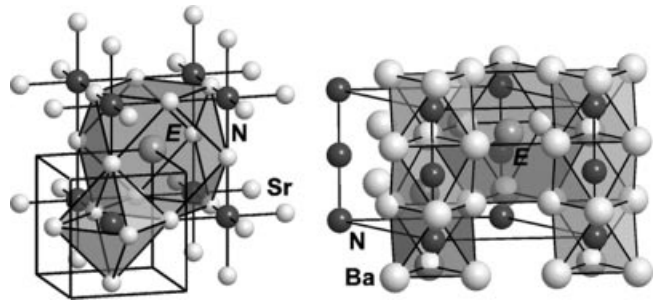

Figure 2 Structure representations of compounds $(Sr_3N)E$ (E = Sb, Bi) resembling a cubic perovskite (left) and $(Ba_3N)E$ (E = Sb, Bi) crystallizing in a hexagonal anti-$BaNiO_3$ structure (right). Crystallographic unit cells are indicated.

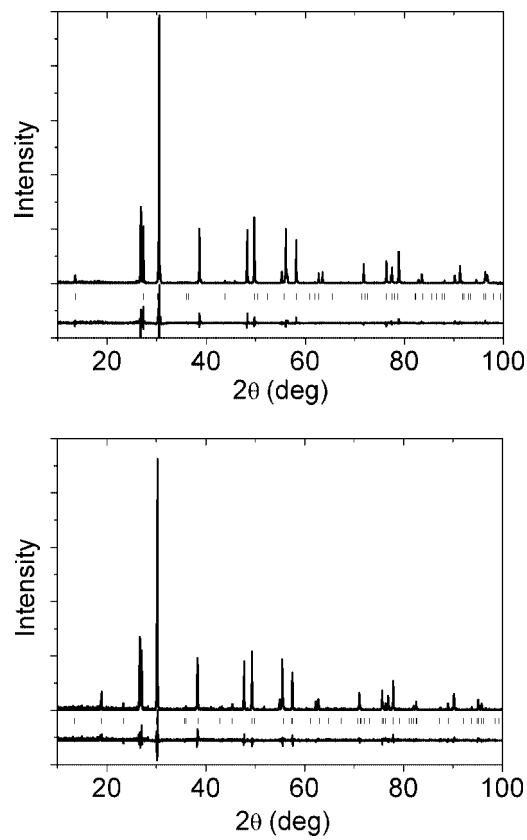

Figure 3 X-ray powder diffraction patterns (CuKα_1 radiation) of (top) $(Ba_3N)Sb$ and (bottom) $(Ba_3N)Bi$. The measured data are shown as points, the continuous line represents the calculated profile and the lower line shows the difference between the calculated and observed intensities. The marks below the data indicate the positions of the reflections.

gain typically is not completed at T_{max} = 1300 K, but continues on cooling. The endothermal effect at T = 1172 K might be related to the peritectic temperature of Sr_3Sb_2 (Sr_5Sb_3). On cooling no significant thermal effect was observed. Above T > 1300 K the weight decreased substantially. Interestingly, the DTA/TG experiments with sample amounts of about 100 mg typically resulted in single phase products according to XRD if the maximum temperature was chosen below T = 1300 K.

The title compounds adopt anti-perovskite type arrangements with nitrogen in octahedral coordination by six alkaline-earth metal ions and group 15 elements in the resulting voids of this framework. Cubic anti-perovskite nitrides with group 15 elements have previously been reported for the systems $(Ca_3N)E$ with E = P, As, Sb, Bi [5] and $(Mg_3N)E$ with E = As, Sb [7]. While $(Sr_3N)Sb$ and $(Sr_3N)Bi$ represent cubic anti-perovskites ($Pm\bar{3}m$, No. 221, Z = 1, Sb: a = 517.25(2) pm, V = 138.390(8) · 10^6 pm^3, Bi: a = 520.691(8) pm, V = 141.170(4) · 10^6 pm^3), $(Ba_3N)Sb$ and $(Ba_3N)Bi$ crystallize in a hexagonal anti-perovskite variant of the $BaNiO_3$ structure type ($P6_3/mmc$, No. 194, Z = 2, Sb: a = 753.33(3) pm, c = 664.45(3) pm, V = 326.56(2) · 10^6 pm^3, Bi: a = 761.28(4) pm, c = 668.05(3) pm, V = 335.30(2) · 10^6 pm^3). Structure representations are depicted in Figure 2. For the determination of the Ba position in the hexagonal unit cell (site 6*h*; x, $-x$ $^1/_4$), and thus interatomic distances, Rietveld refinements on the basis of the X-ray powder patterns for the hexagonal compounds $(Ba_3N)E$ were performed. Figure 3 shows the experimental diffraction patterns together with the calculated profiles and the difference curves of the observed and the simulated patterns as determined by least squares refinements. Table 1 gathers the structure data of all four compounds $(A_3N)E$ including the Ba positional parameters.

Distances d(Sr−N) = 258.63(1) pm (Sb), 260.346(4) pm (Bi) and d(Ba−N) = 267.26(7) pm (Sb), 267.7(1) pm (Bi) of the perovskite nitrides compare well to those in subnitrides with nitrogen species in octahedral coordination: Sr_2N (261 pm) [24] and Ba_3N (273 pm) [25]. For the Sb containing phases distances d(Sb−Sr) = 365.75(2) pm and d(Sb−Ba) = 376.77(6) pm, 401.51(4) pm are longer than those in, e. g., Sr_2Sb [26]: d(Sb−Sr) = 333 pm − 359 pm and Ba_2Sb [27]: d(Sb−Ba) = 353 pm − 375 pm. Similar is true for the Bi containing perovskites: d(Bi−Sr) = 368.18(1) pm, Sr_2Bi [27]: d(Bi−Sr) = 338 pm − 359 pm and d(Bi−Ba) = 380.7(1) pm, 405.56(5) pm, Ba_2Bi [26]:

Table 1 X-ray powder diffraction data for compounds $(A_3N)E$ with A = Sr, Ba and E = Sb, Bi, including results of Rietveld refinements on $(Ba_3N)Sb$ and $(Ba_3N)Bi$.

		$(Sr_3N)Sb$	$(Sr_3N)Bi$	$(Ba_3N)Sb$	$(Ba_3N)Bi$
No. of structural parameters		0	0	4	4
Unit cell parameters	*a*/pm			753.36(1)	761.11(2)
Rietveld	*c*/pm			664.310(6)	667.919(8)
Unit cell parameters	*a*/pm	517.25(2)	520.691(8)	753.33(3)	761.28(4)
Guinier	*c*/pm			664.45(3)	668.05(3)
Space group		$Pm\bar{3}m$, No. 221		$P6_3/mmc$, No. 194	
Positional and displacement parameters:					
A		$^1/_2$, $^1/_2$, 0		0.1605(1), $-x$, $^1/_4$	0.1605(1), $-x$, $^1/_4$
				$B_{iso} = 0.08(3) \times 10^{-4}$ pm^2	$B_{iso} = 0.56(5) \times 10^{-4}$ pm^2
E		0, 0, 0		$^1/_3$, $^2/_3$, $^3/_4$	$^1/_3$, $^2/_3$, $^3/_4$
				$B_{iso} = 0.11(7) \times 10^{-4}$ pm^2	$B_{iso} = 0.44(5) \times 10^{-4}$ pm^2
N		$^1/_2$, $^1/_2$, $^1/_2$		0, 0, 0	0, 0, 0
				$B_{iso} = 0.9(7) \times 10^{-4}$ pm^2	$B_{iso} = 2.0(9) \times 10^{-4}$ pm^2
$R_{profile}$, R_{Bragg}				0.070, 0.071	0.077, 0.088

Table 2. Interatomic distances/pm in hexagonal anti-perovskites $(Ba_3N)E$ (E = Sb, Bi) and related compounds [25, 28] within octahedra (A_6N) and shortest distances between centers of octahedra occupied by nitride ions.

Compound	$(Ba_3N)Sb$	$(Ba_3N)Bi$	Ba_3N	$Na(Ba_3N)$
d(N−N)	332.180(4)	334.047(5)	352.5	349.0
d(Ba−N)	267.26(7)	267.7(1)	272.6	273.4
d(Ba−Ba_{lat})	362.7(1)	362.3(2)	360.2	364.5
d(Ba−Ba_{long})	392.66(5)	394.14(8)	409.3	407.5
d(Ba−E)	376.77(6)	380.7(1)		
	401.51(4)	405.56(5)		

Table 3. Interatomic distances/pm in cubic anti-perovskites $(Sr_3N)E$ (E = Sb, Bi).

Compound	$(Sr_3N)Sb$	$(Sr_3N)Bi$
d(Sr−N)	258.63(1)	260.346(4)
d(Sr−Sr)	365.75(2)	368.18(1)
d(Sr−E)	365.75(2)	368.18(1)

d(Bi−Ba) = 356 pm − 378 pm. Selected distances are gathered in Tables 2 and 3. For the cubic perovskites no indications for a distortion from cubic metric could be obtained from XRD patterns. Distortions of the cubic unit cell to an orthorhombic one (space group *Pnma*) were observed for the comparatively small species of P and As in combination with Ca−N frameworks [5], and for analogues oxides with Si and Ge [9, 12].

The hexagonal perovskite crystal structure can only be expected for compounds containing alkaline-earth metal species with large radii, since the resulting distance d(N−N) and the Coulomb repulsion between N^{3-} in face-sharing octahedra has to be considered. Apparently, for $(Ba_3N)Sb$ the resulting distance d(N−N) = 332.180(4) pm is sufficiently long. However, the octahedra A_6N are elongated along [001]. Similar arguments apply to (Ba3N)Bi: Even though the distance d(N−N) = 334.047(5) pm is slightly longer than in the Sb compound, the octahedra Ba_6N are elongated to the same degree within the error of the Rietveld refinements of the respective X-ray powder diffraction patterns. Remarkably, rods of face-sharing octahedra $^1_\infty[NA_{6/2}]$ also occur in the respective binary compound Ba_3N [25]. Due to the absence of E species these rods are rotated along [001] compared to the ternary nitrides, such that Ba species realize the motif of a hexagonal close packing, while in the ternary nitrides Ba and E together form this motif. Although the distance d(N−N) = 352.5 pm is significantly longer in Ba_3N than in the hexagonal anti-perovskites $(Ba_3N)Sb$ and $(Ba_3N)Bi$, the octahedra in Ba_3N exhibit a considerably higher degree of distortion, i. e., elongation along [001]. The distances within the octahedra indicate smaller and less distorted octahedra for the ternary compounds. Distances in the crystal structures of these compounds are summarized in table 2. As a metallic subnitride isotype of the hexagonal perovskite nitrides $Na(Ba_3N)$ contains Na on the site of E and also highly elongated octahedra [28]. Apparently, the distance d(Ba−N) is the shortest for the Sb containing compound, closely followed by the Bi compound, and is elongated in the metallic compounds Ba_3N and $Na(Ba_3N)$ according to the higher electron concentration at the (Ba_3N) subunit.

The magnetic susceptibilities $\chi = M/H$ of powder samples of the four compounds are displayed in Figure 4. Corrections were applied for the minor effect of some ferromagnetic impurities in the samples (0.2 to $2 \cdot 10^{-5}$ g(Fe)/g calculated for metallic iron). All four compounds are clearly diamagnetic. The temperature dependence of the respective susceptibility can be described by the sum of a temperature independent diamagnetic term (χ_0) of the compound plus a term from small paramagnetic impurities, $\chi(T) = \chi_0 + C/(T-\Theta)$ with $\chi_0 = -54(10)$, $-83(10)$, $-82(15)$, $-97(10) \cdot 10^{-6}$ emu/mol for $(Sr_3N)Sb$, $(Sr_3N)Bi$, $(Ba_3N)Sb$, and $(Ba_3N)Bi$, respectively. Diamagnetic increments for the closed shell configurations of the A^{2+} and E^{5+} ions were taken from [29] and summed up (χ_{core}). There exist differences $\Delta\chi = \chi_0 - \chi_{core} \approx +10 \times 10^{-6}$ emu/mol for the Sr compounds and $\Delta\chi \approx +40 \times 10^{-6}$ emu/mol for the Ba compounds. While $\Delta\chi$ for the Sr compounds is insignifi-

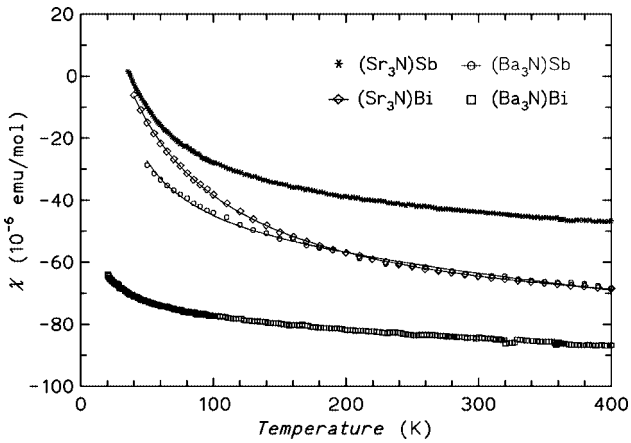

Figure 4 Magnetic susceptibility of $(A_3N)E$ (A = Sr, Ba; E = Sb, Bi) as function of the temperature.

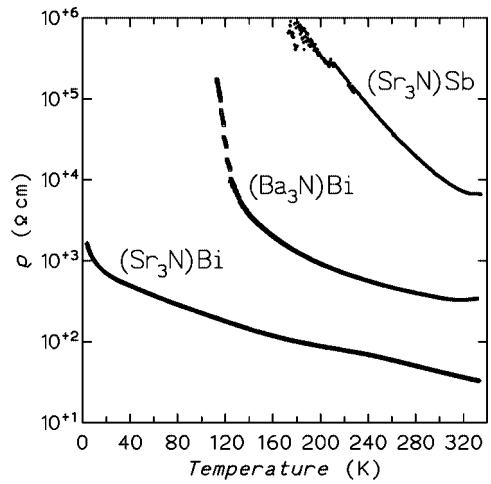

Figure 5 Electrical resistivity of $(Sr_3N)Sb$ and $(A_3N)Bi$ (A = Sr, Ba) as function of the temperature.

cant, for the Ba compounds a small temperature independent or Pauli-paramagnetic contribution seems to be present. In magnetization measurements at small fields (H = 10 Oe) no phase transitions were observed above T = 1.8 K.

The magnitudes and the temperature dependencies of the electrical resistivities $\rho(T)$ (Figure 5) of $(Sr_3N)Sb$, $(Ba_3N)Sb$, and $(Ba_3N)Bi$ are that of intrinsic semiconductors. The resistivity of $(Sr_3N)Bi$ already exceeded 10^6 Ω cm at ambient temperature. From the measurement results all samples can be considered to be highly doped. Therefore, a calculation of the band gap from $\rho(T)$ gives unreliably small values. For $(Sr_3N)Sb$ a band gap of ΔE= 0.2 eV (corresponds to $\Delta E/k_B \approx 2500$ K) can be estimated from the resistivity data. Obviously, the Bi containing compounds are also intrinsic semiconductors and the detected minor paramagnetic contributions do not stem from an electronic density of states at the Fermi level. This conclusion is confirmed by electronic structure calculations.

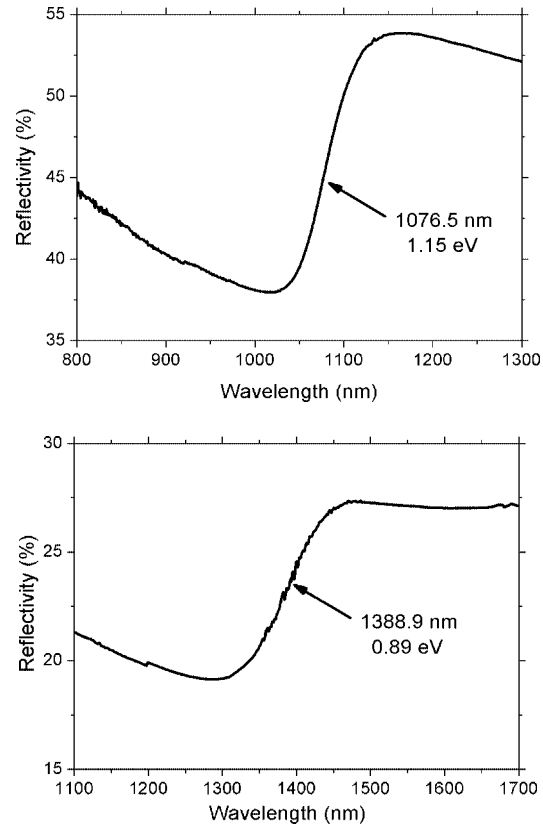

Figure 6 Diffuse reflectivity of (top) $(Sr_3N)Sb$ and (bottom) $(Sr_3N)Bi$ depending on the radiation wavelength. The band gap is indicated.

For $(Sr_3N)Sb$ and $(Sr_3N)Bi$ the band gaps were determined by a diffuse reflectivity technique. The measurement results are shown in Figure 6. The observed values of ΔE = 1.15 eV and ΔE = 0.89 eV, respectively, are compatible with the findings from electrical resistivity measurements and from theory.

The resulting densities of states (DOS) for $(Sr_3N)Bi$ (cubic structure type) and $(Ba_3N)Bi$ (hexagonal structure type) from electronic structure calculations are shown in Figures 7a and 7b, respectively. The DOS for the corresponding Sb compounds are almost identical (not shown) with quantitative changes of only few percent. All calculations result in insulating behavior with band gaps of about ΔE = 0.15 eV and ΔE = 0.5 eV for the cubic and the hexagonal compounds, respectively. This is in qualitative agreement with the experimental observations, although the sizes of the gaps are underestimated as well known for all LDA calculations. The insulating behavior of the $(A_3N)E$ (A = Sr, Ba; E = Sb, Bi) compounds can be understood in a simplified picture of closed shell ions $(A^{2+})_3(N^{3-})(E^{3-})$ resulting in band insulators. The band structure plots in Figure 8 display direct gaps at the Γ point of the Brillouin zone which should correspond to the experimentally observed optical gaps.

The calculated DOS for $(Sr_3N)Bi$ compares well with the data for $(Ca_3N)Bi$ [6]. Besides the deep lying rather lo-

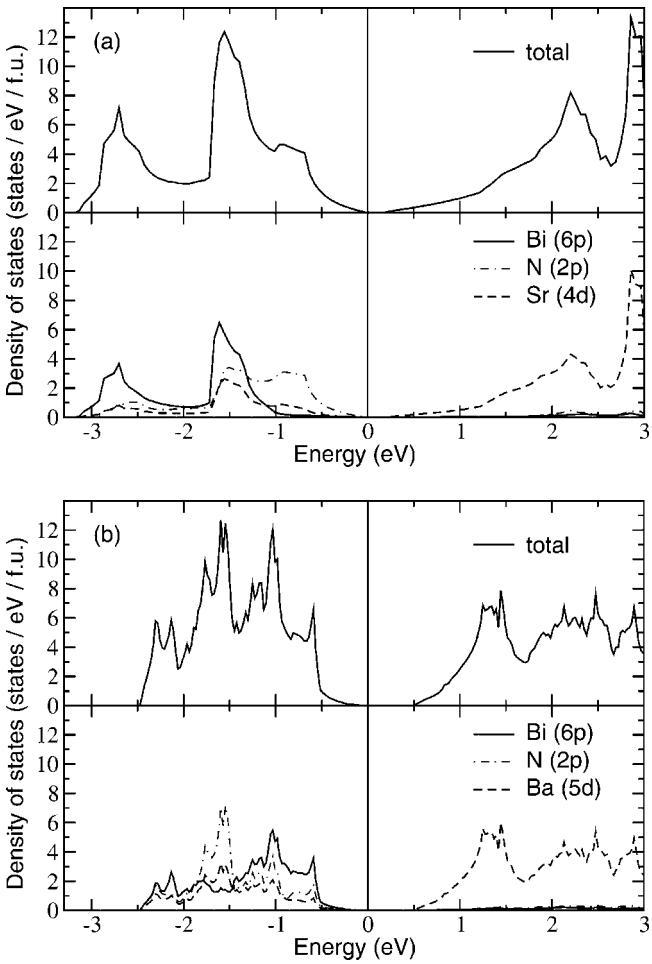

Figure 7 Total and partial density of states per formula unit for (top) $(Sr_3N)Bi$, (bottom) $(Ba_3N)Bi$. The Fermi level is located at zero energy.

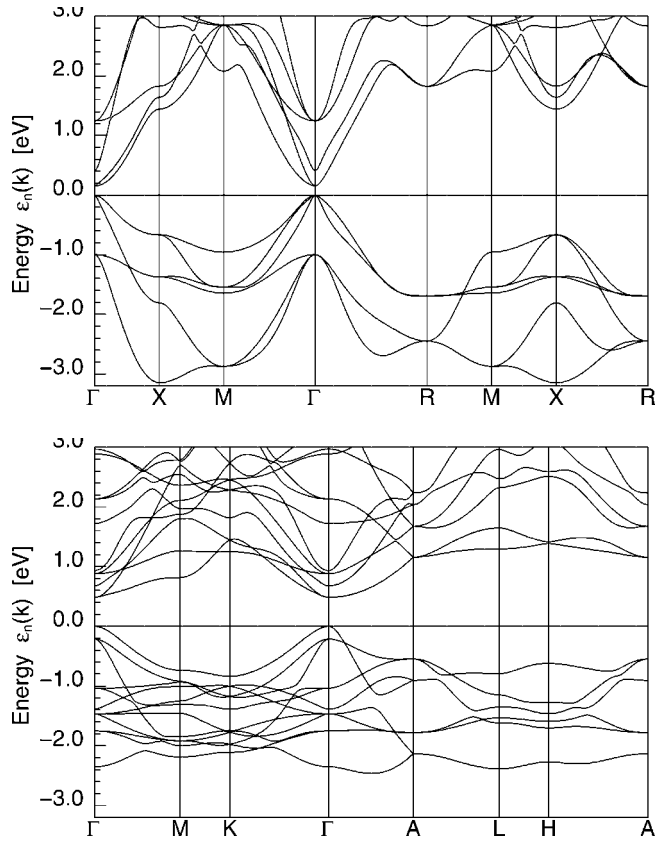

Figure 8 Band structures of (top) $(Sr_3N)Bi$ (cubic perovskite), (bottom) $(Ba_3N)Bi$ (hexagonal perovskite). The Fermi level is at zero energy, the symmetry points are given in the standard notation for the cubic and the hexagonal cell, respectively.

calized N(2*s*) and Bi(6*s*) states at about −11 and −10 eV (not shown), the main contribution to the valence band stems from N(2*p*), Bi(6*p*) and Sr(4*d*) states. These states strongly hybridize with each other in the energy region below the Fermi level down to about −3 eV. The conduction band is mainly composed from Sr(4*d*) states (see Figure 7a). For the hexagonal $(Ba_3N)E$ compounds, the upper part of the valence band is considerably narrower than in the cubic case (compare Figures 7a and b) due to a decreased admixture of N(2*p*) states to the bands close to the Fermi level and an upward shift in energy of the *E*(*p*) states resulting in an increased admixture of these states to the corresponding bonds compared with the cubic cases. A more detailed relation between the crystal structure and the electronic structure, especially the occurrence of the hexagonal structure for the Ba compounds, deserves further investigation and will be published elsewhere.

In summary, the new ternary nitrides of the general composition $(A_3N)E$ (A = Sr, Ba; E = Sb, Bi) crystallize in two structure types governed by the alkaline-earth metal species. Semiconducting properties were predicted from electronic structure calculations and observed by a variety of physical measurement techniques. Chemical bonding is characterized in a simplified picture as ionic with significant orbital mixing.

Acknowledgement. We thank *Steffen Hückmann* for the collection of the diffraction data, *Anja Völzke* for performing the chemical analyses, *Ralf Koban* for operating the SQUID and preparing the resistivity measurements, and *Prof. Dr. R. Kniep* for his constant interest and support.

References

[1] R. Niewa, H. Jacobs, *Chem. Rev.* **1996**, *96*, 2053.
[2] R. Kniep, *Pure Appl. Chem*. **1997**, *69*, 185.
[3] R. Niewa, F. J. DiSalvo, *Chem. Mater*. **1998**, *10*, 2733.
[4] J. Jäger, D. Stahl, P. C. Schmidt, R. Kniep, *Angew. Chem*. **1993**, *105*, 738; *Angew. Chem. Int. Ed*. **1993**, *32*, 709.
[5] M. Y. Chern, D. A. Vennos, F. J. DiSalvo, *J. Solid State Chem.* **1992**, *96*, 415.
[6] R. Niewa, W. Schnelle, F. R. Wagner, *Z. Anorg. Allg. Chem.* **2001**, *627*, 365.
[7] E. O. Chi, W. S. Kim, N. H. Hur, D. Jung, *Solid State Commun.* **2002**, *121*, 309.
[8] D. A. Papaconstantopoulos, W. E. Pickett, *Phys. Rev. B* **1992**, *45*, 4008.

[9] B. Huang, J. D. Corbett, *Z. Anorg. Allg. Chem.* **1998**, *624*, 1787.
[10] A. Widera, H. Schäfer, *Mat. Res. Bull.* **1980**, *15*, 1805.
[11] C. Röhr, *Z. Kristallogr.* **1995**, *210*, 781.
[12] R. Türck, Ph D Thesis, Universität Stuttgart, Germany, 1996.
[13] P. R. Vansant, P. E. Camp, V. E. Van Doren, J. L. Martins, *phys. status solidi B* **1996**, *198*, 87.
[14] P. R. Vansant, P. E. Van Camp, V. E. Van Doren, J. L. Martins, *Phys. Rev. B* **1998**, *57*, 7615.
[15] P. R. Vansant, P. E. Van Camp, V. E. Van Doren, J. L. Martins, *Comp. Mater. Sci.* **1998**, *10*, 298.
[16] I. R. Shein, A. L. Ivanovskii, *Russ. J. Inorg. Chem*. **2003**, *48*, 711; *Zhur. Neo. Khim.* **2003**, *48*, 801.
[17] M. Barberon, R. Madar, E. Fruchart, G. Lorthioir, R. Fruchart, *Mater. Res. Bull*. **1970**, *5*, 1.
[18] R. Benz, W. H. Zachariasen, *Acta Crystallogr.* B **1970**, *26*, 823.
[19] T. B. Massalski (Ed.): Binary Alloy Phase Diagrams. 2nd Ed., ASM International, Materials Park, Ohio 1990.
[20] a) T. Roisnel, J. Rodriguez-Carvajal, *WinPLOTR*, version May 2000: Materials Science Forum, Proceedings of the 7th European Powder Diffraction Conference 2000, Barcelona, Spain, p. 188 b) J. Rodriguez-Carvajal, *FULLPROF.2k*, version 1.6; 2000, Laboratoire Léon Brillouin: 2000. In Abstract of Satellite Meeting on Powder Diffraction, Congress of the International Union of Crystallography, Toulouse, France, 1990, p. 127.
[21] K. Koepernik, H. Eschrig, *Phys. Rev. B* **1999**, *59*, 1743.
[22] J. P. Perdew, Y. Wang, *Phys. Rev. B* **1992**, *45*, 13244.
[23] H. Eschrig: Optimized LCAO Method and the Electronic Structure of Extended Systems, Springer, Berlin, 1989.
[24] N. E. Brese, M. O'Keeffe, *J. Solid State Chem.* **1990**, *87*, 134.
[25] U. Steinbrenner, A. Simon, *Z. Anorg. Allg. Chem*. **1998**, *624*, 228.
[26] R. M. Ripoll, A. Haase, G. Brauer, *Acta Crystallogr*. **1973**, *29*, 1715.
[27] B. Eisenmann, K. Deller, *Z. Naturforsch.* **1975**, *30b*, 66.
[28] P. E. Rauch, A. Simon, *Angew. Chem*. **1992**, *104*, 1505; *Angew. Chem. Int. Ed*. **1992**, *31*, 1519.
[29] P. W. Selwood: Magnetochemistry, Interscience, New York, 2nd Ed., 1956.

